Wiener reconstruction of undersampled imagery

Samuel T. Thurman* and James R. Fienup

The Institute of Optics, University of Rochester, Rochester, New York 14627, USA
*Corresponding author: thurman@optics.rochester.edu

We derive a Fourier-domain Wiener filter for the reconstruction of undersampled imagery. The filter differs from previous implementations in that it permits adjustment of the trade-offs between sharpness of the reconstruction, noise amplification, and aliasing artifact suppression. Additionally, a net transfer function that characterizes the combined effects of the imaging system and the reconstruction process is derived. This net transfer function is valid for both unaliased and aliased spatial frequencies. The expression for the net transfer function is applicable to more general linear image sharpening algorithms. © 2009 Optical Society of America

OCIS codes: 070.2615, 100.1830, 100.2980, 100.3020, 110.4280, 110.4850.

1. INTRODUCTION

The Wiener filter [1–4] is widely used in the reconstruction of imagery sampled at or above the Nyquist limit [5,6]. The Wiener filter requires accurate knowledge of the system optical transfer function, but has several advantages. It is optimum in the sense that it yields a reconstruction with the minimum expected mean-square error based on the object and noise statistics. Being linear, it is computationally efficient and requires just one convolution operation to compute the reconstruction. In some circumstances, the Wiener filter can yield reconstructions of the same quality or better than more complex, nonlinear, iterative algorithms [7].

Many imaging systems, however, operate below the Nyquist limit due in part to signal-to-noise and field-of-view considerations [8]. While a Wiener filter applicable to undersampled imagery has been derived previously in the spatial domain [4], we present a Fourier-domain derivation. While the Fourier-domain treatment does have limitations (it does not apply to space-variant imaging conditions and becomes considerably more complicated when the object and/or noise statistics are nonstationary), there are a number of advantages. In the Fourier domain, it is easy to separate the terms representing the unaliased and aliased portions of the image and the noise. This being done, filter parameters can be introduced to control the trade-offs between the sharpness of the reconstruction, noise amplification, and the suppression of aliasing artifacts. Additionally, the Fourier-domain analysis yields an expression for a net transfer function that represents the combined effects of the imaging system and the reconstruction process at both unaliased and aliased spatial frequencies. This net transfer function is a nontrivial generalization of the well-known result for Wiener filtering Nyquist sampled data, for which the net transfer function is simply the product of the imaging system transfer function and the Fourier-domain Wiener filter. Previous spatial-domain work on using the Wiener filter with undersampled data did not yield this result. The net transfer function is a vital tool for assessing the overall performance of the system and can be used to compute various image quality metrics [9,10]. For example, [11] uses the net transfer function to calculate the relative edge response of an undersampled imaging system.

A mathematical model for undersampled imagery is described in Section 2. The Wiener filter for undersampled imagery is derived in Section 3. An expression for the net system transfer function after reconstruction is given in Section 4. An example with simulated imagery is discussed in Section 5. Section 6 is a summary.

2. IMAGING MODEL

For notational convenience, all of the equations in Sections 2–4 will be written in one dimension; the extension to two dimensions is straightforward. Assuming space-invariant imaging conditions, the incoherent image $i(x)$ of an object $o(x)$ is given by the convolution

$$i(x) = s(x) \otimes o(x), \tag{1}$$

where $s(x)$ is the system incoherent impulse response or point-spread function (PSF). A digitally sampled version of this image can be written as

$$h_m = i(m\Delta x) = \int_{-\infty}^{\infty} i(x)\delta(x - m\Delta x)\mathrm{d}x, \tag{2}$$

where the subscript $m \in \{-M/2, (2-M)/2, \ldots, (M-2)/2\}$ is an image-domain sample index, M is the total number of samples, Δx is the sample spacing, and $\delta(x)$ is the Dirac delta function. In practice, there is noise in the measurement of h_m. Thus, a noisy version of the digital image can be written as

$$g_m = h_m + n_m, \tag{3}$$

where n_m are additive noise samples. The discrete Fourier transform (DFT) of g_m is given by

$$G_p = \frac{1}{\sqrt{M}} \sum_{m=-M/2}^{M/2-1} g_m \exp\left(-i2\pi \frac{mp}{M}\right), \tag{4}$$

where the subscript $p \in \{-M/2, (2-M)/2, \ldots, (M-2)/2\}$ is a Fourier-domain sample index, $i = (-1)^{1/2}$, and the spacing between samples in the Fourier domain is

$$\Delta u = \frac{1}{M\Delta x}. \tag{5}$$

Using Eqs. (1)–(5), the Fourier-domain samples G_p can be written as [12]

$$G_p = N_p + \frac{1}{\sqrt{M}\Delta x} \sum_{k=-\infty}^{\infty} \int_{-\infty}^{\infty} \left\{ [S(u)O(u)] \right.$$

$$\left. \otimes \frac{1}{\Delta u}\mathrm{sinc}\left(\frac{u - kM\Delta u}{\Delta u}\right) \right\} \delta(u - p\Delta u) \mathrm{d}u, \tag{6}$$

where the uppercase variables represent the Fourier-domain counterparts to the corresponding lowercase variables, and $\mathrm{sinc}(x) = \sin(\pi x)/(\pi x)$. Equation (6) can be written as the sum of three distinct terms as

$$G_p = N_p + H_{a,p} + H_{0,p}, \tag{7}$$

where N_p is the noise, $H_{a,p}$ is the aliased portion of the Fourier transform of the image,

$$H_{a,p} = \frac{1}{\sqrt{M}\Delta x} \sum_{\substack{k=-\infty \\ k \neq 0}}^{\infty} \int_{-\infty}^{\infty} \left\{ [S(u)O(u)] \right.$$

$$\left. \otimes \frac{1}{\Delta u}\mathrm{sinc}\left(\frac{u - kM\Delta u}{\Delta u}\right) \right\} \delta(u - p\Delta u) \mathrm{d}u$$

$$\approx \frac{1}{\sqrt{M}\Delta x} \sum_{\substack{k=-\infty \\ k \neq 0}}^{\infty} S[(p - kM)\Delta u] O[(p - kM)\Delta u], \tag{8}$$

and $H_{0,p}$ is the unaliased portion of the Fourier transform

$$H_{0,p} = \frac{1}{\sqrt{M}\Delta x} \int_{-\infty}^{\infty} \left[S(u)O(u) \right.$$

$$\left. \otimes \frac{1}{\Delta u}\mathrm{sinc}\left(\frac{u}{\Delta u}\right) \right] \delta(u - p\Delta u) \mathrm{d}u$$

$$\approx \frac{1}{\sqrt{M}\Delta x} S(p\Delta u) O(p\Delta u). \tag{9}$$

The sinc convolutions in the above equations, which arise from the truncation of the image by the width of the detector array, have three effects: (i) to introduce coordinate translations of $kM\Delta u$ [in Eq. (8) only], (ii) to limit the resolution of H_p to approximately Δu, and (iii) to cause spectral leakage proportional to the amplitude of the sinc function sidebands, converting the finite-support spectrum $S(u)O(u)$ to a spectrum with infinite support [but typically having small values outside the support of $S(u)$]. Ignoring (ii) and (iii) yields the approximate expressions on the third lines of Eqs. (8) and (9).

3. WIENER FILTER

The Wiener reconstruction of the object can be written in the Fourier domain as

$$\hat{F}_p = W_p G_p, \tag{10}$$

where W_p is the Wiener filter. The Wiener filter is specified to yield the minimum expected mean-square error between the reconstruction and the original object based on the noise and object statistics, both of which are assumed to be stationary. When aliasing is present, this error is calculated with respect to the unaliased portion of the object Fourier transform, i.e., we wish to find W_p that minimizes

$$\langle e \rangle = \left\langle \frac{1}{M} \sum_{p=-M/2}^{M/2-1} |W_p G_p - F_p|^2 \right\rangle, \tag{11}$$

where the angle brackets indicate an expectation value calculated with respect to both the noise and object statistics and

$$F_p = \frac{1}{\sqrt{M}\Delta x} \int_{-\infty}^{\infty} \left[O(u) \otimes \frac{1}{\Delta u}\mathrm{sinc}\left(\frac{u}{\Delta u}\right) \right] \delta(u - p\Delta u) \mathrm{d}u$$

$$\approx \frac{1}{\sqrt{M}\Delta x} O(p\Delta u) \tag{12}$$

represents an unaliased discrete version of the Fourier transform of the original object. Substituting Eq. (7) into Eq. (11) yields

$$\langle e \rangle = \frac{1}{M} \sum_{p=-N/2}^{N/2-1} [|W_p^2|(\langle |N_p|^2\rangle + \langle N_p H_{a,p}^*\rangle + \langle N_p^* H_{a,p}\rangle + \langle |H_{a,p}|^2\rangle$$

$$+ \langle N_p H_{0,p}^*\rangle + \langle N_p^* H_{0,p}\rangle + \langle H_{a,p} H_{0,p}^*\rangle + \langle H_{a,p}^* H_{0,p}\rangle$$

$$+ \langle |H_{0,p}|^2\rangle) - W_p(\langle N_p F_p^*\rangle + \langle H_{a,p} F_p^*\rangle + \langle H_{0,p} F_p^*\rangle)$$

$$- W_p^*(\langle N_p^* F_p\rangle + \langle H_{a,p}^* F_p\rangle + \langle H_{0,p}^* F_p\rangle) + \langle |F_p|^2\rangle]. \tag{13}$$

If the noise is zero-mean and independent of the object statistics, the cross-terms involving N_p with $H_{a,p}$, $H_{0,p}$, or F_p vanish. Also, the cross-terms involving $H_{a,p}$ with $H_{0,p}$ and those involving $H_{a,p}$ with F_p vanish due to the following property of $O(u)$

$$\langle O(u)O^*(u')\rangle = \Phi_o(u)\delta(u - u'), \tag{14}$$

where $\Phi_o(u)$ is the spectral density or power spectrum of the object, which results from the object stationarity assumption [13]. The only remaining term that varies from the standard Wiener filter derivation [3] is $\langle |H_{a,p}^2|\rangle$, which can be evaluated as

$$\langle |H_{a,p}^2|\rangle \approx \frac{1}{M\Delta x^2} \sum_{\substack{k=-\infty \\ k \neq 0}}^{\infty} \sum_{\substack{k'=-\infty \\ k' \neq 0}}^{\infty} S[(p - kM)\Delta u]S^*[(p - k'M)\Delta u]$$

$$\times \langle O[(p - kM)\Delta u]O^*[(p - k'M)\Delta u]\rangle$$

$$\approx \frac{1}{M\Delta x^2} \sum_{\substack{k=-\infty \\ k \neq 0}}^{\infty} |S[(p - kM)\Delta u]|^2 \Phi_o[(p - kM)\Delta u]$$

$$\equiv \frac{1}{M\Delta x^2}\Phi_a(p\Delta u), \tag{15}$$

where $\Phi_a(u)$ represents the aliased portion of the image power spectrum,

$$\Phi_a(u) = \sum_{\substack{k=-\infty \\ k \neq 0}}^{\infty} |S(u - kN\Delta u)|^2 \Phi_o(u - kN\Delta u). \tag{16}$$

Thus, the expected mean-square error can be written as

$$\langle e \rangle \approx \frac{1}{M^2\Delta x^2} \sum_{p=-M/2}^{M/2-1} \{|W_p^2|[\Phi_n(p\Delta u) + \Phi_a(p\Delta u)]$$
$$+ [|W_p^2||S(p\Delta u)|^2 - W_pS(p\Delta u) - W_p^*S^*(p\Delta u) + 1]$$
$$\times \Phi_o(p\Delta u)\}, \tag{17}$$

where $\Phi_n(u)$ is the noise power spectrum, defined by

$$\langle |N_p|^2 \rangle = \frac{1}{M\Delta x^2}\Phi_n(p\Delta u). \tag{18}$$

Solving for the Wiener filter that minimizes E yields

$$W_p = \frac{S^*(p\Delta u)\Phi_o(p\Delta u)}{|S(p\Delta u)|^2\Phi_o(p\Delta u) + c_n\Phi_n(p\Delta u) + c_a\Phi_a(p\Delta u)}, \tag{19}$$

where c_n and c_a are parameters that have been introduced to allow for trade-offs between sharpness, noise, and aliasing artifacts in the reconstruction $\hat{F}_p$. The true minimum $\langle e \rangle$ solution is for $c_n = c_a = 1$. Comparing this expression with the traditional Fourier-domain Wiener filter [3], the term representing aliasing $\Phi_a(p\Delta u)$ appears as an additional noise term. When there is no aliasing, i.e., $\Phi_a(p\Delta u) = 0$, Eq. (19) reduces to the form of a Wiener–Helstrom filter without aliasing.

4. NET SYSTEM TRANSFER FUNCTION

Note that the Wiener filter can be written as a sampled version of a continuous function $\Omega(u)$, i.e.,

$$W_p = \int_{-\infty}^{\infty} \Omega(u)\delta(u - p\Delta u)du = \Omega(p\Delta u), \tag{20}$$

where $\Omega(u)$ is a periodic function defined as

$$\Omega(u) = \begin{cases} \dfrac{S^*(u)\Phi_o(u)}{|S(u)|^2\Phi_o(u) + c_n\Phi_n(u) + c_a\Phi_a(u)} & \text{for } \dfrac{-M\Delta u}{2} \leq u < \dfrac{M\Delta u}{2} \\ \Omega(u - M\Delta u) & \text{otherwise} \end{cases}. \tag{21}$$

Using Eqs. (7)–(10), (20), and (21), the reconstruction $\hat{F}_p$ can be written as

$$\hat{F}_p = W_p(N_p + H_{a,p} + H_{0,p}) \approx W_pN_p + \frac{1}{\sqrt{M}\Delta x}\sum_{k=-\infty}^{\infty} W_pS[(p - kM)\Delta u]O[(p - kM)\Delta u]$$

$$= W_pN_p + \frac{1}{\sqrt{M}\Delta x}\sum_{k=-\infty}^{\infty}\int_{-\infty}^{\infty} \Omega(u)S(u)O(u)\delta[u - (p - kM)\Delta u]du. \tag{22}$$

It is evident from this equation that the net system transfer function, after Wiener filtering, is given by

$$S_{net}(u) = \Omega(u)S(u), \tag{23}$$

which can be written as

$$S_{net}(u) = \frac{S(u)S^*(u - kM\Delta u)\Phi_o(u - kM\Delta u)}{|S(u - kM\Delta u)|^2\Phi_o(u - kM\Delta u) + c_n\Phi_n(u - kM\Delta u) + c_a\Phi_a(u - kM\Delta u)}$$

$$\text{for } \left(k - \frac{1}{2}\right)M\Delta u \leq u < \left(k + \frac{1}{2}\right)M\Delta u \quad \text{and all } k \in \{0, \pm 1, \pm 2, \dots\}. \tag{24}$$

Figure 1(a) illustrates the system transfer function $S(u)$ for an undersampled imaging system, in which Δx is a factor of 8/3 larger than the Nyquist sample spacing [the diffraction-limited cutoff frequency is $4/(3\Delta x)$]. The vertical dashed lines represent the range of spatial frequencies for which the Nyquist sampling condition is satisfied. Figure 1(b) shows a representative periodic extension of the Wiener filter $\Omega(u)$. The portion of $\Omega(u)$ between the dashed lines represents the Wiener filter W_p that would actually be used to reconstruct the image. Figure 1(c) shows the net system transfer function $S_{net}(u)$, equal to the product of $S(u)$ and $\Omega(u)$, which is valid at both unaliased and aliased spatial frequencies. Note that Eq. (23) is valid for any linear sharpening kernel, e.g., generic 3 × 3 and 5 × 5 sharpening kernels, as well as the Wiener filter, when $\Omega(u)$ is replaced by the periodic extension of the DFT of said kernel.

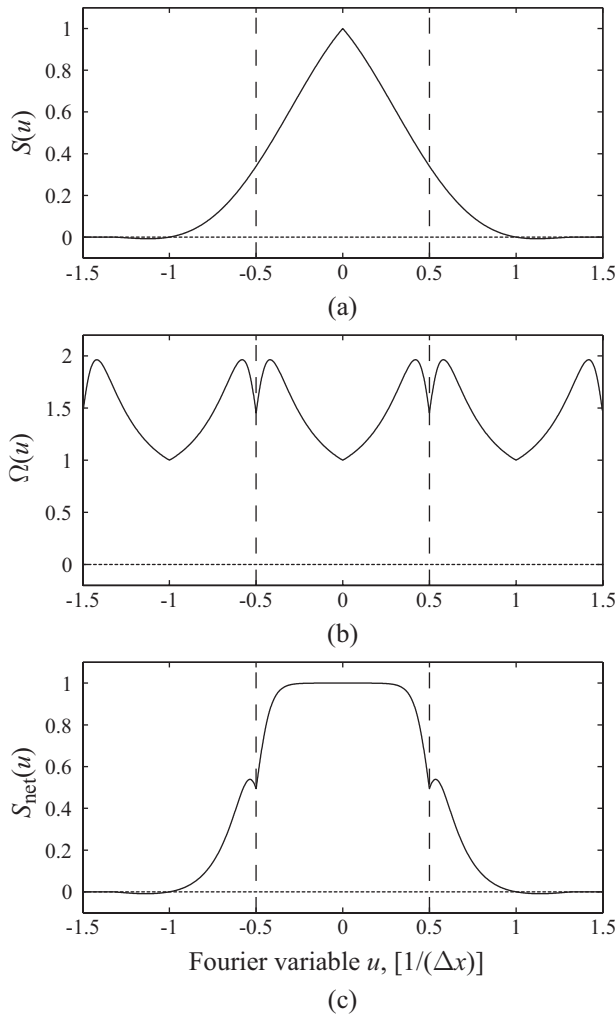Figure 2 provides further insight into the interpreta-

Fig. 1.   Diagram illustrating Fourier-domain contributions to the net system transfer function: (a) the unaliased transfer function of the imaging system $S(u)$, (b) the periodically extended version of the Wiener filter $\Omega(u)$, and (c) the unaliased net system transfer function $S_{\mathrm{net}}(u)$. The vertical dashed lines indicate the extent of the unaliased portion of the Fourier domain, $|u| < 1/(2\Delta x)$.

tion of $S_{\mathrm{net}}(u)$. The following two sequences yield the same final image: (i) passing the object data through the transfer function of the imaging system $S(u)$, sampling, and reconstructing with Wiener filter W_p, and (ii) passing the object data through the net transfer function $S_{\mathrm{net}}(u)$ and sampling. Either process yields the same result, even with aliasing. Note that the addition of noise is omitted from these steps, as $S_{\mathrm{net}}(u)$ does not apply to the noise.

5. EXAMPLE IMPLEMENTATION

Figure 3 shows an aerial photograph [14] with a 7.6 cm (3 in.) ground sample distance (GSD) used as the digital object, $o(x,y)$, for this example. Figure 4 shows a simulated 45.7 cm (18 in.) GSD noisy image, $g_{m,n}$, where the system PSF $s(x,y)$ is given by the convolution of the Airy disk pattern for an aberration-free optical system and a small square window representing the spatial area of an individual detector pixel. The sampling ratio [8] was $Q = \lambda f/(D\Delta x) = 0.75$, where λ is the wavelength of light, f is
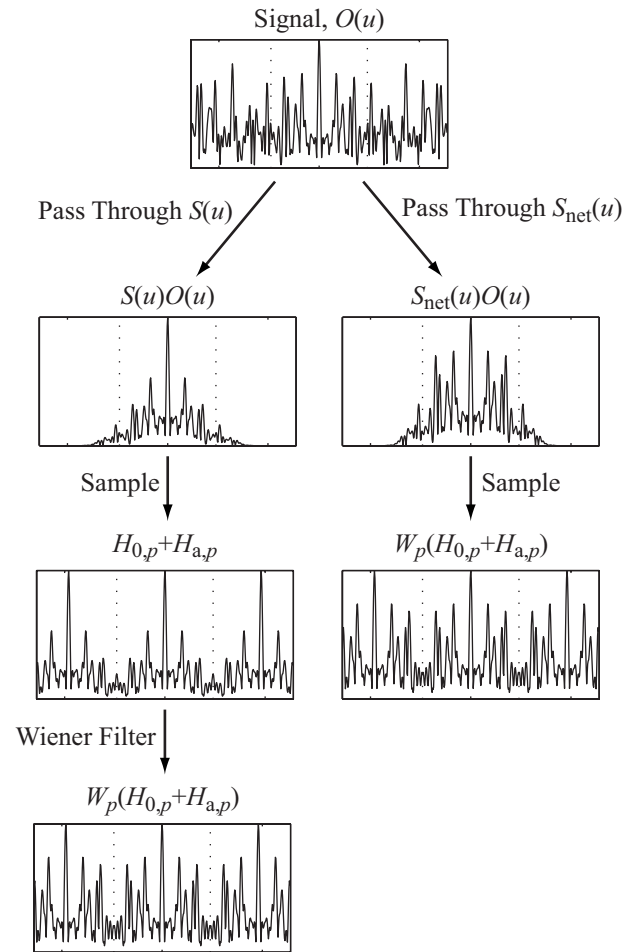

Fig. 2.   Diagram illustrating the interpretation of the net transfer function $S_{\mathrm{net}}(u)$. Passing object data through $S(u)$, downsampling, and reconstructing with W_p (left) yields the same result as passing object data through $S_{\mathrm{net}}(u)$ and downsampling (right).

the system focal length, and D is the pupil diameter. Thus, $g_{m,n}$ is undersampled by a factor of 8/3 in comparison to the Nyquist sampling rate ($Q = 2$ for Nyquist sampling), as was the case for Fig. 1. Both Poisson-distributed shot noise, where the average image signal was

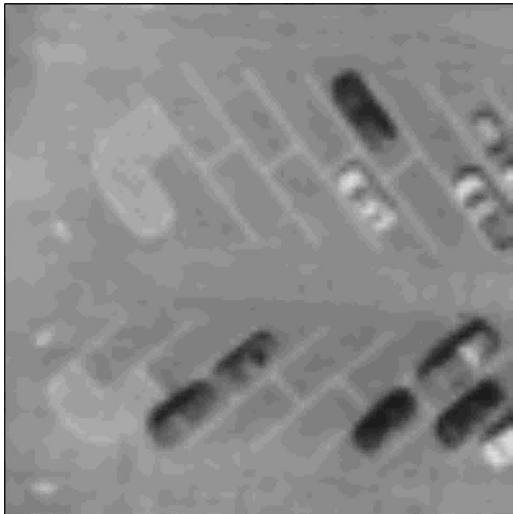Fig. 3.   Digital object [14] used for simulation.

Fig. 4.   Noisy aliased image $g_{\mathrm{m,n}}$.

80,000 photoelectrons/pixel, and Gaussian-distributed detector read noise, with a standard deviation of 20 photoelectrons, were included in $g_{m,n}$. Additionally, 10-bit quantization was applied to $g_{\mathrm{m,n}}$. These conditions are representative of ideal exposure conditions with a realistic detector, yielding a high signal-to-noise ratio image.

Both the object and noise power spectra, $\Phi_{\mathrm{o}}(u,v)$ and $\Phi_{\mathrm{n}}(u,v)$, respectively, are needed for the Wiener filter. Here we switch from 1D to 2D notation. A common model [7,15–20] for the power spectrum of typical objects or secenes is

$$\Phi_{\mathrm{o}}(u,v) = \begin{cases} A_0^2 & \text{for } \rho = 0 \\ A^2 \rho^{-2\alpha} & \text{for } \rho \neq 0 \end{cases}, \tag{25}$$

where $\rho = (u^2+v^2)^{1/2}$ is the radial spatial frequency coordinate and A_0, A, and α are parameters of the model. The corresponding model for the image power spectrum $\Phi_{\mathrm{i}}(u,v)$, including both the unaliased and aliased portions of the noise-free image, is given by

$$\Phi_{\mathrm{i}}(u,v) = \sum_{k=-\infty}^{\infty} \sum_{\ell=-\infty}^{\infty} |S(u - kM\Delta u, v - \ell M\Delta v)|^2$$
$$\times \Phi_{\mathrm{o}}(u - kM\Delta u, v - \ell M\Delta v). \tag{26}$$

Typically, the noise is nearly white [21], such that

$$\Phi_{\mathrm{n}}(u,v) = \Phi_{\mathrm{n}}, \tag{27}$$

is a constant, independent of spatial frequency. Assuming the noisy Fourier-domain samples $|G_{p,q}|^2$ are statistically independent (except for correlations arising from the Hermitian symmetry of $G_{p,q}$) and obey a negative-exponential probability distribution [22] of the form

$$P(|G_{p,q}^2|) = \frac{1}{\Phi_{\mathrm{i}}(p\Delta u, q\Delta v) + \Phi_{\mathrm{n}}} \exp\left[\frac{-|G_{p,q}^2|}{\Phi_{\mathrm{i}}(p\Delta u, q\Delta v) + \Phi_{\mathrm{n}}} \right], \tag{28}$$

then the power spectrum parameters A, α, and Φ_{n} can be estimated from the image data $G_{p,q}$ by maximizing the following log-likelihood function [22,23]
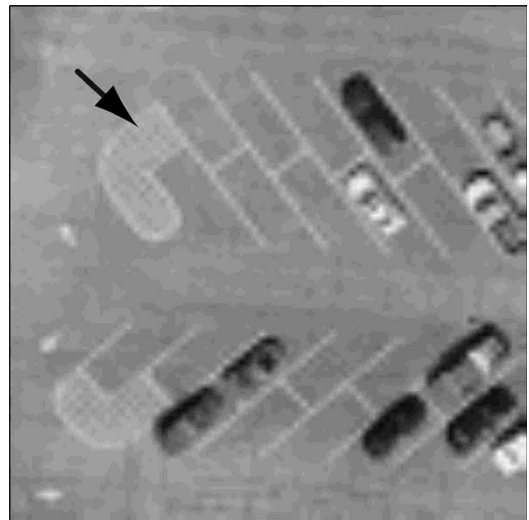
(a)
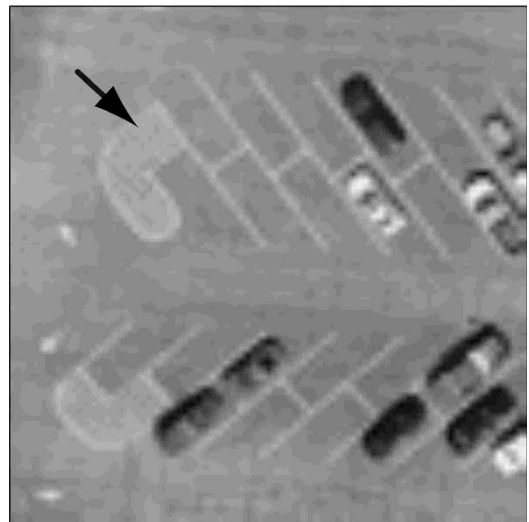
(b)
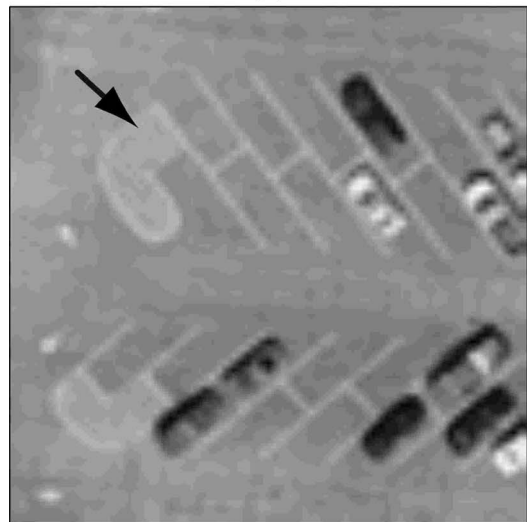
(c)

Fig. 5.   Wiener filter reconstructions $\hat{f}_{m,n}$ of Fig. 4, with $c_{\mathrm{n}} = 1$ and (a) $c_{\mathrm{a}} = 0$, (b) $c_{\mathrm{a}} = 1$, and (c) $c_{\mathrm{a}} = 5$. The arrows indicate a region containing noticeable aliasing artifacts associated with the painted lines of the parking lot; note that the stripes appear to go in the wrong direction.
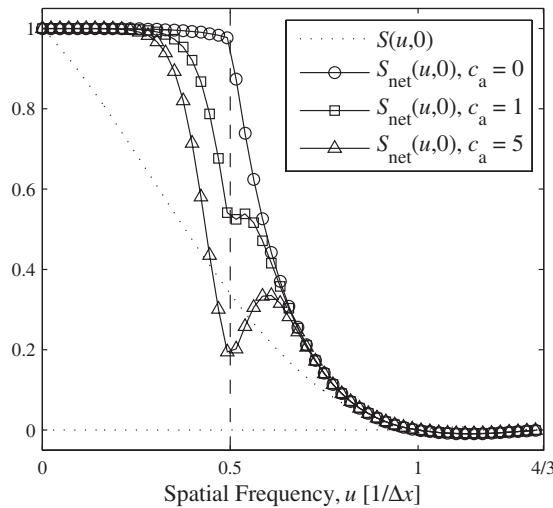
Fig. 6. Net system transfer functions $S_{net}(u,v)$ corresponding to each of the reconstructions shown in Fig. 5. For comparison, the system transfer function before processing $S(u,v)$ is also shown. The vertical dotted lines represent the extent of the unaliased portion of the object Fourier transform, $|u| < 1/(2\Delta x)$.

$$L = \sum_{(p,q) \neq (0,0)} \frac{-|G_{p,q}|^2}{\Phi_i(p\Delta u, q\Delta v) + \Phi_n} - \ln[\Phi_i(p\Delta u, q\Delta v) + \Phi_n].$$

$$(29)$$

Additionally, $A_0 = G_{0,0}$ can be used to evaluate the object power spectrum at the dc spatial frequency. Note that the $M\Delta x^2$ factors appearing in Eqs. (15) and (18) have been dropped from Eqs. (28) and (29) for notational convenience as they do not affect the maximization of L.

Figure 5 shows Wiener filter reconstructions for the example imagery using object and noise power spectra estimates, resulting from the method described above, and filter parameter values $c_n = 1$ and $c_a = 0$, 1, and 5. These reconstructions demonstrate the trade-off between sharpness and the suppression of aliasing artifacts (e.g., the "staircasing" effect on the tilted edges and the periodic lines on the pavement appearing to go the wrong way) associated with the value of c_a. Figure 5(a) appears visually to be the sharpest, while Fig. 5(c) is the least sharp, being only marginally sharper than the unprocessed image shown in Fig. 4. However, the aliasing artifacts in the region indicated are most noticeable in Fig. 5(a) and least noticeable in Fig. 5(c). Figure 6 shows $S_{net}(u,0)$ for each case. Note that for $c_a = 0$, the Wiener filter boosts $S_{net}(u)$ up to near unity for all the unaliased spatial frequencies $|u| < 1/(2\Delta x)$, since the signal-to-noise ratio is high. As the value of c_a increases, however, the amount of boosting of $S_{net}(u)$ is reduced to provide better suppression of aliasing artifacts, at the expense of reduced edge sharpness in the reconstruction.

6. SUMMARY

We have derived a Fourier-domain Wiener filter for aliased imagery. Filter parameters were introduced to control the trade-offs of edge sharpness, noise amplification, and aliasing artifact suppression. An expression for the net system transfer function $S_{net}(u,v)$ after applica-

tion of the Wiener filter (or any other linear filter) was derived. This expression for $S_{net}(u,v)$ is a vital tool for the analysis of overall system performance (including the effects of both the imaging system and the reconstruction algorithm). Finally, an example implementation of the Wiener filter was demonstrated. This example illustrated the trade-off between image sharpness and aliasing artifacts associated with the filter parameter c_a.

REFERENCES

1. N. Wiener, *Extrapolation, Interpolation and Smoothing of Stationary Time Series* (Wiley, 1950).
2. H. W. Bode and C. E. Shannon, "A simplified derivation of linear least square smoothing and prediction theory," Proc. IRE **38**, 417–425 (1950).
3. C. W. Helstrom, "Image reconstruction by the method of least squares," J. Opt. Soc. Am. **57**, 297–303 (1967).
4. A. K. Jain, *Fundamentals of Digital Image Processing* (Prentice Hall, 1989).
5. H. Nyquist, "Certain topics in telegraph transmission theory," Trans. Am. Inst. Electr. Eng. **47**, 617–644 (1928).
6. E. T. Whittaker, "On the functions which are represented by the expansions of the interpolation theory," Proc. R. Soc. Edinburgh **35**, 181–194 (1915).
7. J. R. Fienup, D. Griffith, L. Harrington, A. M. Kowalczyk, J. J. Miller, and J. A. Mooney, "Comparison of reconstruction algorithms for images from sparse-aperture systems," Proc. SPIE **4792**, 1–8 (2002).
8. R. D. Fiete, "Image quality and λFN/*p* for remote sensing systems," Opt. Eng. **38**, 1229–1240 (1999).
9. J. C. Leachtenauer, W. Malila, J. Irvine, L. Colburn, and N. Salvaggio, "General image-quality equation: GIQE," Appl. Opt. **36**, 8322–8328 (1997).
10. P. G. J. Barten, *Contrast Sensitivity of the Human Eye and Its Effects on Image Quality* (SPIE, 1999), Chap. 8.
11. S. T. Thurman and J. R. Fienup, "Wiener filtering of aliased imagery," Proc. SPIE **7076**, 70760J (2008).
12. See the Appendix of S. T. Thurman and J. R. Fienup, "Signal-to-noise ratio trade-offs associated with coarsely sampled Fourier transform spectroscopy," J. Opt. Soc. Am. A **24**, 2817–2821 (2007).
13. L. Mandel and E. Wolf, *Optical Coherence and Quantum Optics* (Cambridge U. Press, 1995), p. 59.
14. This image is in the public domain and is available through the URL http://seamless.usgs.gov/.
15. N. G. Deriugin, "The power spectrum and the correlation function of the television signal," Telecommunications **1**, 1–12 (1956).
16. G. J. Burton and I. R. Moorhead, "Color and spatial structure in natural scenes," Appl. Opt. **26**, 157–170 (1987).
17. D. J. Field, "Relations between the statistics of natural images and the response properties of cortical cells," J. Opt. Soc. Am. A **4**, 2379–2394 (1987).
18. D. J. Tolhurst, Y. Tadmor, and T. Chao, "Amplitude spectra of natural images," Ophthalmic Physiol. Opt. **12**, 229–232 (1992).
19. D. L. Ruderman and W. Bialek, "Statistics of natural images: scaling in the woods," Phys. Rev. Lett. **73**, 814–817 (1994).
20. A. van der Schaaf and J. H. van Hateren, "Modelling the power spectra of natural images: statistics and information," Vision Res. **36**, 2759–2770 (1996).
21. R. L. Lucke, "Fourier-space properties of photon-limited noise in focal plane array data, calculated with the discrete Fourier transform," J. Opt. Soc. Am. A **18**, 777–790 (2001).
22. D. R. Gerwe, M. Jain, B. Calef, and C. Luna, "Regularization for non-linear image restoration using a prior on the object power spectrum," Proc. SPIE **5896**, 21–36 (2005).
23. S. T. Thurman and J. R. Fienup, "Noise histogram regularization for iterative image reconstruction algorithms," J. Opt. Soc. Am. A **24**, 608–617 (2007).